Wind and Structures, *Vol. 19, No. 6 (2014) 603-621*
DOI: http://dx.doi.org/10.12989/was.2014.19.6.603

Finite-element modeling of a light-framed wood roof structure

Ryan B Jacklin, Ashraf A. El Damatty* and Ahmed A. Dessouki

Department of Civil and Environmental Engineering, The University of Western Ontario, London, Ontario Canada, N6A 5B9

(Received March 15, 2014, Revised September 20, 2014, Accepted October 8, 2014)

Abstract. Past high speed wind events have exposed the vulnerability of the roof systems of existing light-framed wood structures to uplift loading, contributing greatly to economic and human loss. This paper further investigates the behaviour of light-framed wood structures under the uplift loading of a realistic pressure distribution. A three-dimensional finite-element model is first developed to capture the behaviour of a recently completed full-scale experiment. After describing the components used to develop the numerical model, a comparison between the numerical prediction and experimental results in terms of the deflected shape at the roof-to-wall connections is presented to gain confidence in the numerical model. The model is then used to analyze the behaviour of the truss system under realistic and equivalent uniform pressure distributions and to perform an assessment of the use of the tributary area method to calculate the withdrawal force acting on the roof-to-wall connections.

Keywords: wood structures; structural behaviour; finite element; wind damage

1. Introduction

Residential light-framed wood structures are very common in North America due to the ease of construction, the low cost, and the availability of materials and labour. The use of repetitive wood member, sheathing panels, and non-structural elements results in a structure with a high degree of redundancy, as well as complex and indeterminate load paths. Typical residential wood structures, subject to span and live load limits, are not analyzed by an engineer. Instead member sizes and connections details follow the prescriptive requirements of the local governing building code. Past extreme wind events have exposed the vulnerability of this type of structure to the uplift loading that results from high winds, with the sheathing-to-truss (STT) connections and the roof-to-wall (RTW) connections being identified as the most critical connections in the load path (FEMA 1993, Shanmugam *et al*. 2009). The damage that resulted to light-framed wood structures represented a large portion of the US$20-25 billion of economic loss that was caused by Hurricane Andrew in 1992 (HUD 1993). Approximately 95% of this loss resulted from failures of materials of the roof system (Baskaran and Dutt 1997). While light-framed wood structures performed much better during Hurricane Katrina in 2005, the lack of a continuous load path from the roof to the foundation was still found to result in structural damage leading to economic loss (van de Lindt *et al*. 2007).

*Corresponding author, Professor, E-mail: damatty@uwo.ca

Copyright © 2014 Techno-Press, Ltd.
http://www.techno-press.org/?journal=was&subpage=8 ISSN: 1226-6116 (Print), 1598-6225 (Online)

As extreme wind events expose the vulnerabilities of existing structures, building codes change to improve the capacity of new structures. For example, the most recent edition of the National Building Code of Canada defined high wind areas, in which the capacity required for both the STT and the RTW connections are increased above that of the previous edition (NRC 2010). Recent changes have also occurred to the Florida Building Code. Major improvements were made to the South Florida Building Code following Hurricane Andrew. These changes were adopted locally in 1994 before becoming standard for the entire state of Florida in 2001 (Gurley *et al*. 2006). As building codes are improved, existing structures remain with known vulnerabilities, as they are built to the standard of an outdate code. Structures built before 1994 in the coastal regions of the United States are extremely vulnerable to the uplift forces caused by wind as the majority use insufficient nails for the STT connections (Datin *et al*. 2011). The large economic loss which has occurred, the frequent building code changes, and the vulnerability of existing structures all demonstrate the need to better understand the behaviour of light-framed wood structures in high speed wind events.

In an attempt to better understand the behaviour of light-framed wood structures under uplift loading, researchers have used a combination of experimental and numerical studies. Morrison *et al*. (2012) loaded a full-scale structure built to the provisions of the Ontario Building Code with a realistic pressure distribution. The loading, which was developed from a wind tunnel study, was simulated using a system of 58 pressure bags, resulting in a spatially and temporally varying roof sheathing pressure. They found that the structure demonstrated significant load sharing, resulting in tributary area loads on the RTW connections that were significantly above the failure loads anticipated from experiments on individual toe-nail connections. Under the peak pressures of the realistic pressure distribution, the RTW connections were found to suffer permanent withdrawal, becoming increasingly damaged as the experimental loading progressed to higher wind velocities. This connection damage was confirmed in the individual connection testing completed by Morrison and Kopp (2011). The realistic wind loading applied during this study was unique, as previous studies had focused on the behaviour of the toe-nail connection under ramp loading. The testing of the individual connections found that permanent withdrawal occurred under the peak loads. During the unloading and reloading phases after damage, the stiffness of the connection remained similar to that of the initial stiffness of the connection.

Zisis and Stathopoulos (2012) studied the behaviour of an as-built, gable-style light-framed wood structure under environmental loading. The structure was implemented with load cells between the walls and foundation. Pressure taps on the structure and local weather monitoring stations provided information about the magnitude of the applied wind loading. The study found that approximately 30% of the total applied uplift force was transferred through the gable walls to the foundation. The experimental study was complemented with the dynamic analysis of a finite-element model consisting of frame, area and rigid link elements. Due to the energy dissipation within the structure, the wind load acting on the foundation was approximately 17 to 28 % less experimentally than predicted by the numerical model.

Shivarudrappa and Nielson (2013) developed a finite-element model of a gable roof structure, validated using the experimental work of Datin and Prevatt (2013). Linear frame and shell elements were used with nonlinear link elements to capture the behaviour of the structure. The model was used to study the sensitivity of the distribution of the applied load at the RTW connections on the properties of the materials and connections within the structure. The sensitivity analysis found that the stiffness of the RTW connections had a large effect on the load sharing behaviour of the structure. Increasing the stiffness of the RTW connections reduced the amount of

applied load shared to surrounding trusses. Increasing the bending stiffness of the sheathing was found to increase the load shared between the trusses. The study also found that the additional RTW connections created along the gable end truss reduced the forces acting on the RTW connections of the next closest truss.

Li *et al*. (1998) created a finite-element model of a truss system using the commercial software ETABS. The trusses were modeled using frame elements with increased bending stiffness for the top chord members to capture the partially composite behaviour created by the sheathing. The behaviour of the sheathing was captured using beam elements. The moment transferred by the gusset plate connection between truss members was neglected. The developed model showed good agreement with the experimental results presented in previous literature in terms of deflection, member axial force, and load distribution.

This paper further investigates the behaviour of light-framed wood structures under the uplift loading of a realistic pressure distribution. A three-dimensional finite-element model is first developed to capture the behaviour of a recently completed full-scale experiment. After describing the components used to develop the numerical model, a comparison between the numerical prediction and experimental results in terms of the deflected shape at the RTW connections is presented to gain confidence in the numerical model. The model is then used to analyze the behaviour of the truss system under realistic and equivalent uniform pressure distributions and to perform an assessment of the use of the tributary area method to calculate the withdrawal force resulting at each RTW connection.

2. Discription of the conducted experiment

An experiment has been recently conducted at the Insurance Research Lab for Better Homes at the University of Western Ontario to study the behaviour of a light-framed wood structure under a realistic wind pressure distribution. The tested structure, shown in Fig. 1, was built to the provisions of the Ontario Building Code (OBC 2006) and inspected to ensure that it matched the typical construction techniques of the area. A realistic pressure distribution was developed from a wind tunnel study and simulated using a system of 58 pressure bags, resulting in an applied pressure to the roof sheathing that varied in both time and space. The pressure bags ranged from 0.36 m^2 to 5.8 m^2 in area. As shown in Fig. 2, the smallest bags were located at the windward edge of the structure, where the largest variation in the magnitude of pressure occurs for the selected wind angle. The magnitude of the realistic pressure distribution that was initially applied to the structure corresponded to a mean wind velocity of 20 m/s at roof height. The wind velocity was increased by 5 m/s until failure of the RTW connections, which occurred under the pressure corresponding to a 45 m/s wind velocity. As the pressures were applied, the resulting deflection at each RTW connection was recorded. Further details of the experimental procedure are available in Morrison *et al*. (2012).

3. Numerical modeling of the roof structure

The experimental structure is numerically modeled using the finite-element program SAP 2000 (Computers and Structures, Inc. 2009). A plan view of the structural skeleton of the roof system is provided in Fig. 3, followed by a description of the various components of the numerical model.

Fig. 1 Full-scale experimental set-up with steel reaction frame (http://www.eng.uwo.ca/irlbh/)

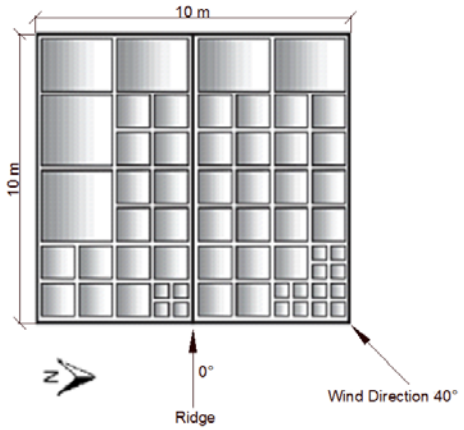

Fig. 2 Plan view of pressure box distribution for the full-scale experiment (Morrison 2010)

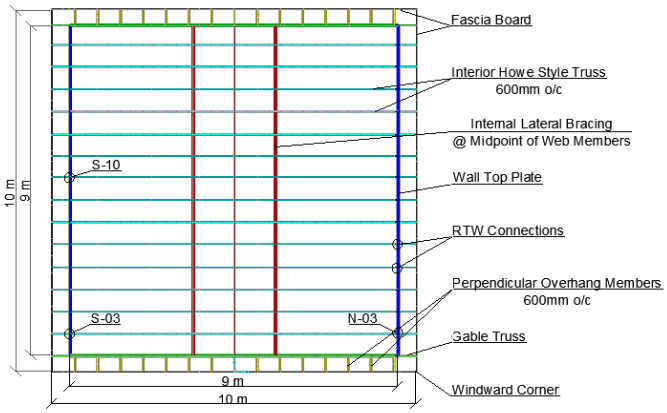

Fig. 3 Plan view of structural skeleton of roof system

3.1 Interior trusses

Linear frame elements are used to model the wood members of the truss system. The structure contains 14 interior, Howe-style trusses spaced at 600 mm (2ft) centers with the dimensions shown in Fig. 4. Top and bottom chords of the trusses are 39 mm x 89 mm (2x4) members. Interior webbing of the trusses are constructed of 39 mm x 64 mm (2x3) members. The material properties for the frame elements are provided by the Canadian Wood Design Manual (CWDM) (CWC and CSA 2010) assuming dry, SPF, No. 1/No. 2 lumber.

Physical connections between the members within each truss are made with metal "gusset" plates. Li *et al*. (1998) conducted numerical modeling of a wood truss system and concluded that neglecting the moment transfer of the gusset plate connection resulted in accurate force distribution within truss members when compared to experimental literature. Moment is assumed to be transferred through a gusset plate when the member is continuous through the connection, as is the case on the top and bottom chords of the truss. Fig. 5 shows the locations of the moment releases applied to the numerical model to capture the behaviour of the truss described by Li *et al*. (1998).

3.2 Gable truss

The two exterior trusses, identified as the gable trusses in Fig. 3, contain modifications when compared to the interior trusses. Each gable truss has additional vertical webbing for the support of the exterior vertical sheathing. Also, as the gable truss is continuously supported by an external wall, extra RTW connections are made along the length of the truss.

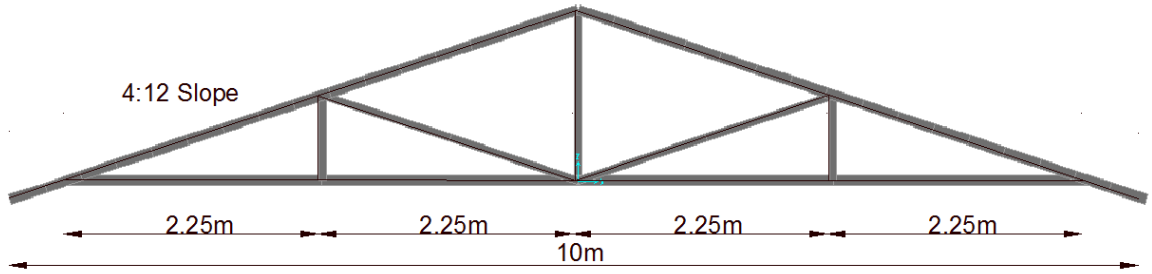

Fig. 4 Elevation view and dimensions of interior Howe-style truss

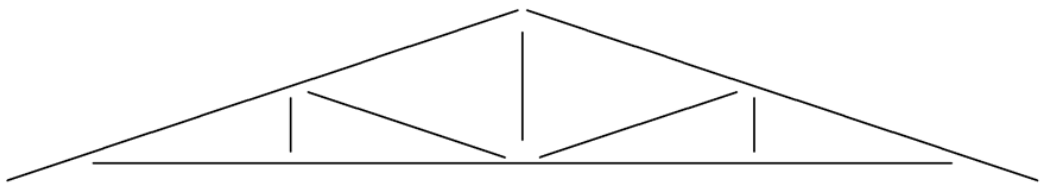

Fig. 5 Moment releases included in the finite-element model

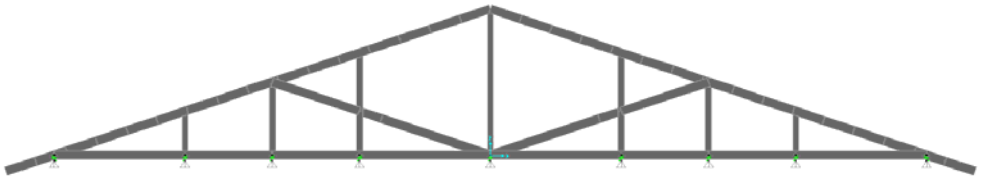

Fig. 6 Gable end trusses of numerical model with additional external RTW connections

Depending on the method of construction, either the vertical sheathing or the additional RTW connections could be the major contributor to the increase in stiffness of the gable end compared to the interior trusses. If the vertical sheathing is continuous past the RWT connection and connected to the wall below, the connection between the roof and the walls would be dependent on nail shear. The uplift behaviour of the gable truss would not rely on the withdrawal capacity of nails and would be extremely rigid relative to the interior roof trusses. In this case, the sheathing would be the primary contributor to the increase in stiffness of the gable truss. If the vertical sheathing is not continuous past the RWT connection, while the sheathing would increase the bending stiffness of the top chord of the truss, it would have negligible effect on the global uplift behaviour of the truss. In this case, the primary contributor to the additional stiffness would be the brick facade or additional RTW connections installed along the length of the truss. The second case is modeled in this paper.

As shown in Fig. 6, four additional vertical members are included in the numerical model of the gable trusses, with additional RTW connections at each location that a vertical member intersects the bottom chord of the truss. Similar to the numerical formulation of the interior trusses, moment releases are applied to each member of the gable trusses unless the member is continuous through the gusset plate connection.

3.3 Plywood sheathing

A total of 2112 shell elements are used to model the plywood sheathing of the roof. Shell elements have membrane and bending capabilities allowing them to deform in and out-of-plane, simulating the realistic behaviour of the sheathing. Each element has an approximate area of .05 m^2. The smallest pressure boxes in the full-scale experiment are represented by 8 area elements in the finite-element model.

Wood is an anisotropic material, with strength dependent on the direction of the grains. The stiffness of plywood sheathing is dependent on the layout of the grains of the plys. To account for this, a modification factor is used to reduce the bending stiffness of the sheathing in the direction perpendicular to the face grains to match the properties given by the CWDM. For 12 mm CSP plywood constructed with 4 plys, the bending stiffness is 9 times larger in the direction of the face grains than that in the direction perpendicular to the face grains (CWC and CSA 2010). Thus, a factor of 0.11 is applied to reduce the bending stiffness of the shell element in this weak axis.

The plywood sheathing increases the bending stiffness of the top chord of the truss as partially composite behaviour occurs and a “T” beam is created. To capture this behaviour, the center line of the shell elements have been offset from the centerline of the top chord of the truss. The nodes of the top chord are connected to the nodes of the sheathing using a body constraint to model composite behaviour.

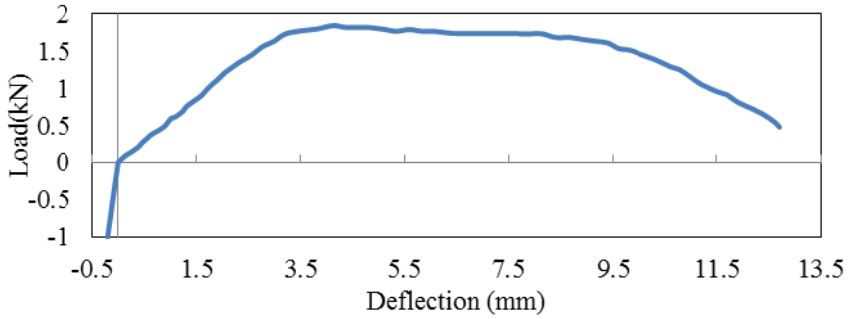

Fig. 7 RTW connection load-deflection relationship

3.4 Roof-to-wall connection

A multi-linear force-deflection relationship is used to simulate the behaviour of the toe-nail connection, captured using a multi-linear elastic link element. A typical load-deflection relationship for a toe-nail connection constructed with three, 8D common nails, shown in Fig. 7, is used in the numerical model. This connection property has been adapted from the experimental work presented by Reed *et al*. (1997). The load deflection curve has a high stiffness when subjected to a negative load, representing the truss bearing on the top plate of the wall. Under withdrawal loading, the connection has an initial stiffness of 550 kN/m, with an ultimate capacity of 1.8 kN.

3.5 Roof overhang

The roof system overhangs the top plate of the walls by approximately 500 mm in each direction. Fig. 4 shows the construction method of the overhang in the direction parallel to the trusses. The top chord of the truss continues past the RTW connection by 500 mm, supporting the sheathing. The numerical model includes a fascia board, shown in Fig. 3, which is a 38 mm by 89 mm (2x4) member running perpendicular to the truss system, connecting the free end of the overhang of each truss.

A 500 mm overhang is included at each gable end. The roof sheathing is supported by 38mm by 89 mm (2x4) members connected perpendicular to the gable truss, identified as the perpendicular overhang members in Fig. 3. A fascia board running parallel to the top chord of the truss is attached to the outer edge of each 38 mm by 89 mm (2x4) member. The fascia board supports the sheathing along the outermost edge of the overhang around the entire structure.

3.6 Boundary conditions

It is assumed that the walls beneath the RTW connections have negligible effect on the deflections recorded experimentally as the members of the walls will experience little axial deformation under the magnitude of loading applied. The wall system is neglected and the boundary conditions of the numerical model are in the form of horizontal and vertical deflection restraints applied immediately beneath the top plate of the exterior walls.

3.7 Load input data

The comparison between the experimental and numerical results is carried out by conducting quasi-static analysis. The natural period of the structure is well below the period of the loading, as such, the dynamic effect should have negligible effect on the behaviour of the truss system. The nonlinear behaviour of the tested structure is found to occur mostly at the RTW connections, where permanent, nonlinear damage occurs as the peak pressures are applied. Before application of the first damaging peak pressure, the behaviour of the connection can be approximated as linear elastic (Morrison and Kopp 2011). As such, the load cases considered for this analysis are selected before the first damaging peak pressure so that nonlinear behaviour of the RTW connections is not anticipated and quasi-static analysis is justifiable. For each selected load case, an instantaneous snap shot of the non-uniform pressure distribution that was applied to the experimental structure is applied to the numerical model. The deflection resulting at the RTW connections at this time is compared to the numerical results assuming no initial deflection. To compare the numerical and experimental results at higher wind levels, after nonlinear damage to the RTW connections has occurred, time-history analysis becomes necessary.

Twelve load cases have been selected from the experiment before damage occurred. The loading of the selected time steps results in the largest global uplift forces applied to the structure before the connections sustain damage. Tables 1 and 2 show the time steps selected from the full-scale experiment to validate the finite-element model. The global uplift force acting on the structure is larger than the dead load of the roof (approximately 15 kN) for each selected pressure distribution.

Two pressure distributions, load case 5 and load case 12, are shown below in Figs. 8 and 9, respectively. The distribution of pressure in load case 5 shows a strong positive pressure in the windward corner, with a nearly uniform negative pressure applied over the remainder of the structure. The distribution of pressure in load case 12 shows a negative pressure applied over the entire roof system with stronger pressures above the east gable end. Load case 12 results in the largest experimental deflections for the critical connection before nonlinear damage initiates. The pressure distributions applied experimentally and numerically neglect the positive pressures acting on the underside of the overhangs.

Table 1 Load case selection from 20 m/s TLP experiment

Load Case	1	2	3	4	5	6
Time in TLP test (sec)	57.10	96.96	279.32	361.48	651.76	755.46
Global Uplift Force (kN)	-21.3	-21.9	-22.3	-27.8	-22.0	-28.9

Table 2 Load case selection from 25 m/s TLP experiment

Load Case	7	8	9	10	11	12
Time in TLP test (sec)	47.76	75.92	95.66	102.66	132.38	166.72
Global Uplift Force (kN)	-30.2	-30.8	-34.5	-30.2	-30.7	-32.4

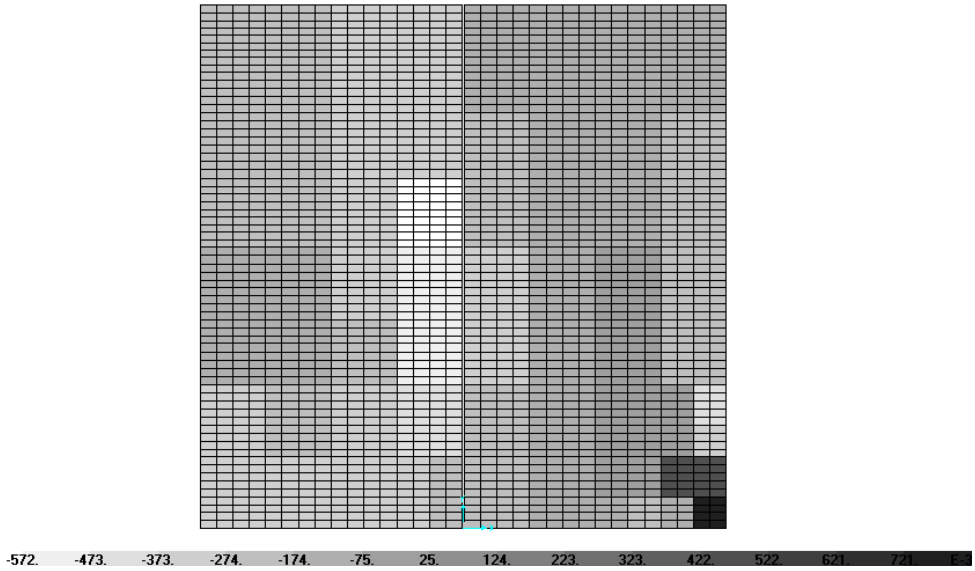

Fig. 8 Pressure distribution for load case 5 (Maximum = 720Pa , Minimum = -570Pa)

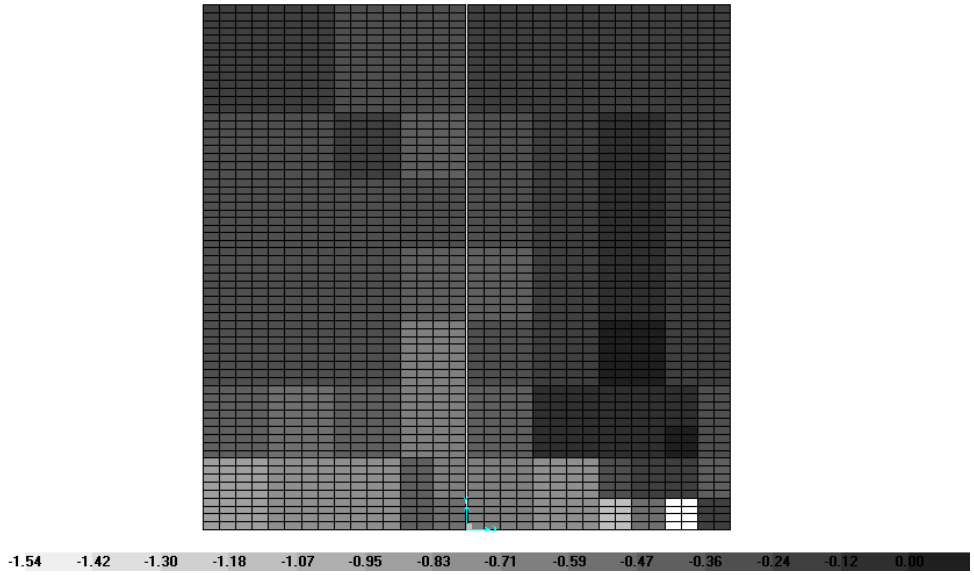

Fig. 9 Pressure distribution for load case 12 (Maximum = 0 kPa, Minimum = -1.54 kPa)

4. Validation of the numerical model

The validation of the finite-element model includes a comparison between the numerical predictions and the experimental full-scale test results in terms of the instantaneous deflection values at the RTW connections. Each RTW connection is labeled as either a north or south link, followed by the truss number. The windward corner is labeled connection N-01, with numbers increasing along the length of the structure. Overhangs are labeled connections N/S-01 and N/S-18. The gable ends are connections N/S-02 and N/S-17. The critical connection during the experiment is identified as S-03.

For validation of the numerical model, the prediction of the deflected shape of the roof should be similar to the full-scale experimental results. Variation of individual connection magnitudes along the length is expected due to the variability of the toe-nail connection properties. The deflection of the RTW connections along the north and south walls is presented for load cases 5 and 12 in Figs. 10 and 11, respectively.

In terms of the deflected shape of the RTW connections along the length building, the prediction of the numerical model shows good agreement with the experimental results. For load case 5, in which the applied pressure is most uniformly distributed, the numerical model predicts a nearly uniform deflected shape along the building. The experimental results show more variability in the deflection of each connection. The average deflection for the south side connections when the roof is subjected to the applied pressure of load case 5 is 0.4 mm for both the numerical prediction and the experimental results. For the deflection of the north connections between connections N-09 and N-17 in Fig. 10, the numerical prediction and experimental results match very well in terms of average, with both having a value of 0.2 mm. The numerical model does not show strong agreement with the global behavior of the structure for connections N-01 to N-07. Despite a difference in magnitude, the model does predict the trend of the deflection in the windward corner.

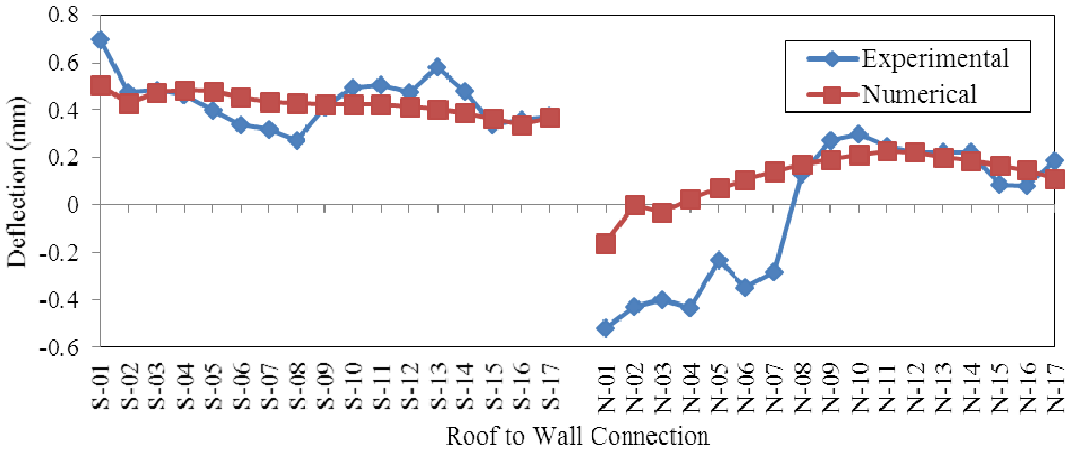

Fig. 10 Deflection of the RTW connections for load case 5

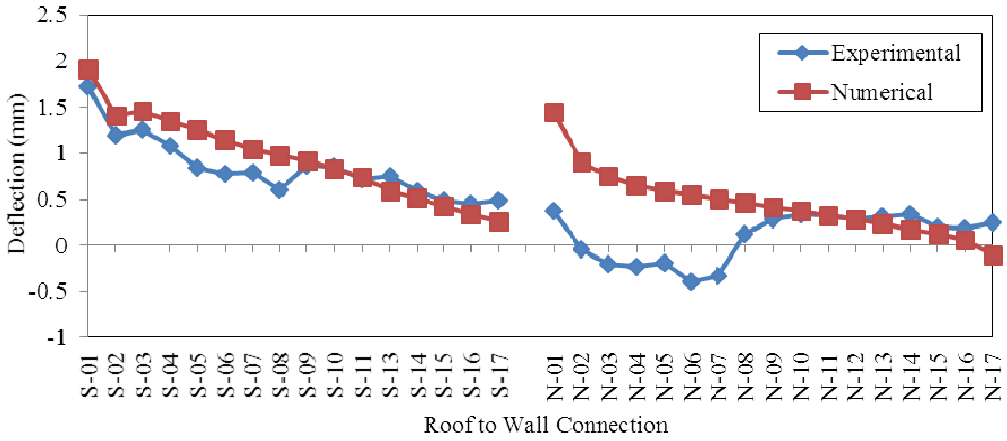

Fig. 11 Deflection of the RTW connections for load case 12

Fig. 11 shows the RTW connection deflection obtained under the applied pressure of load case 12. Under this applied loading, the numerical prediction matches the experimental results very well in terms of magnitude of deflection along the length of the structure. Also, there is strong agreement in the trend of deflection for the connections near the east gable on the south side. Both the numerical prediction and experimental results predict that connection S-02, located on the gable truss, experiences less deflection than the surrounding connections. This local minimum results from the increased stiffness of the gable truss due to the additional RTW connections. Both the numerical prediction and experimental results agree that the global maximum occurs at the overhang of the structure, connection S-01, which has less vertical stiffness than the gable and interior trusses as it is not connected directly to the walls beneath. The numerical prediction and experimental results also show a local maximum at connection S-03, followed by a relatively linear reduction in deflection along the length of the structure. Similar to the results of load case 5, the experimental and numerical deflected shapes have a difference in magnitude for the north connections N-01 to N-07, despite demonstrating a similar deflected shape of the structure. For both cases, the experimental structure experienced a negative deflection for the north-east connections, a behaviour which, except for the overhang connections (N/S-01 and N/S-17), the numerical model is not able to capture due to the assumed load deflection behaviour of the RTW connection and the applied boundary conditions. This difference in deflection is likely due to the nailed connections of the walls of the structure, which were neglected in the numerical model.

During the full-scale experiment, connection S-03 was determined to be the critical link, as it was the location of failure (Morrison 2010). Therefore, it is important that the model matches the behaviour at this connection. The deflection of the connection corresponding to the center truss, S-10 is also presented to validate the model behaviour throughout the twelve selected pressure distributions. The numerical predictions and the experimental results for the deflection of connections S-03 and S-10 throughout the selected load cases are plotted in Figs. 12 and 13.

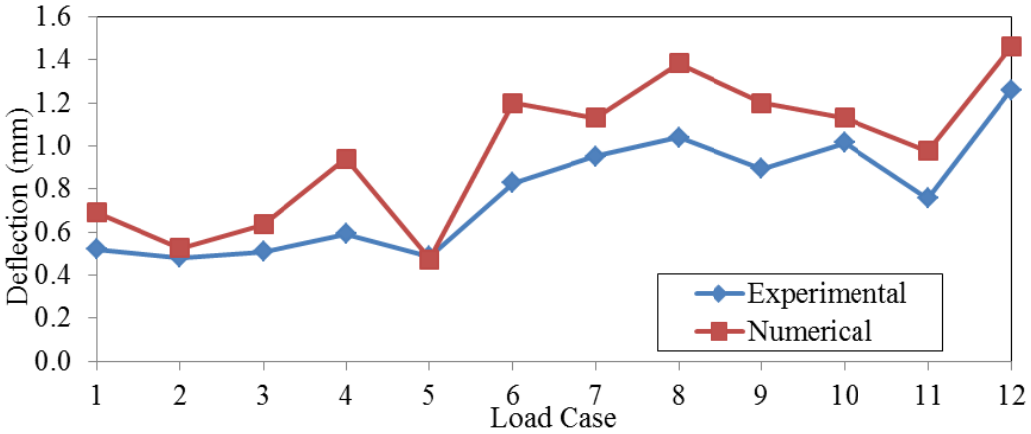

Fig. 12 Deflection of connection S-03 throughout load cases 1 to 12

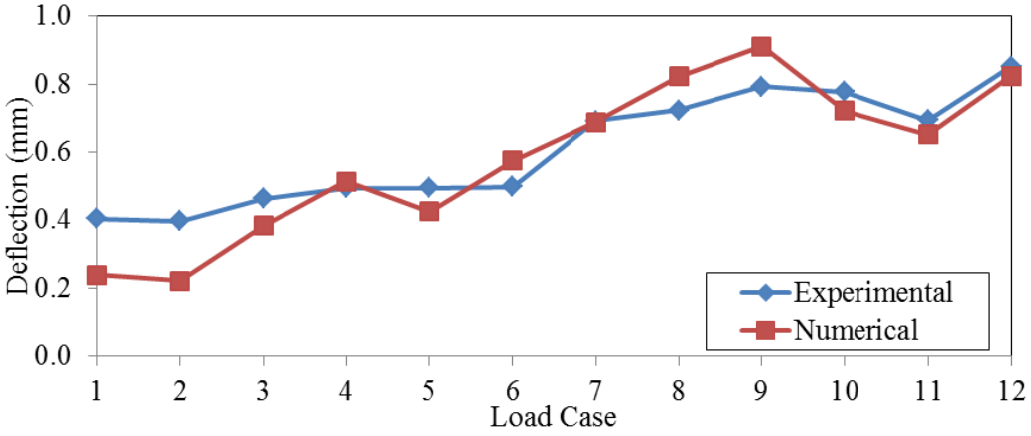

Fig. 13 Deflection of connection S-10 throughout load cases 1 to 12

The numerical model tends to overestimate the deflection at connection S-03 by an average of 26% when compared to the experimental results. The data points which show the best correlation with the experimental data are load cases 1,2,3,5 and 10. In general, these cases tend to have a uniform pressure distribution over the leeward connections, while the other cases tend to have higher peak pressures above this connection. While the model slightly overestimates the deflection at this link, the trend through the load cases is matched very well. The numerical prediction of connection S-10 shows very strong agreement with the experimental results, with an average percent difference of 14%. The largest magnitude of error shown in the deflection of this connection occurs for load cases 1 and 2 when the tributary area loads applied to this truss are the lowest.

In the author's opinion, the general trend of the deflected shape predicted by the finite-element model reasonably matches the experimental results. Considering the variability of the stiffness of a toe-nail connection, the error found is acceptable.

5. Analysis of structural behaviour

5.1 Analysis of the tributary area method

The tributary area method is commonly used to evaluate the forces acting at the RTW connections. The pressure applied to the sheathing by each box is distributed to the nearest supporting trusses assuming that the sheathing is simply supported between trusses, resulting in a line load applied to the top chord of the truss. Each truss is assumed to act independently to transfer the resulting line load to the RTW connections. The width of the tributary area of each truss is half the span to the next truss, roughly 600mm (2ft) for the studied structure. The gable ends have approximately 20% larger tributary area than the interior trusses as they support the entire overhang. The numerical model is used to assess the adequacy of this approach when applied to wood roofs subjected to non-uniform pressure distributions.

Fig. 14 compares the force at the RTW connections predicted by each analysis method under the pressure distribution of load case 12. The tributary area method greatly overestimates the force at connections N-03 and S-03, predicting more than double the force withheld by the RTW connection than the numerical analysis prediction. The difference in magnitude between the prediction of the numerical model and the tributary area method demonstrates the large amount of force that is shared to the gable end truss by the less stiff interior trusses. The numerical model predicts load sharing between the connections on the interior of the structure, since a much more linear distribution of force on the connections occurs along the length of the structure when compared to the tributary area method. The load sharing distributes the pressure over multiple connections, reducing the demand on the individual connections that have the highest tributary area force prediction, while increasing the demand on the connections predicted to withstand lower load levels.

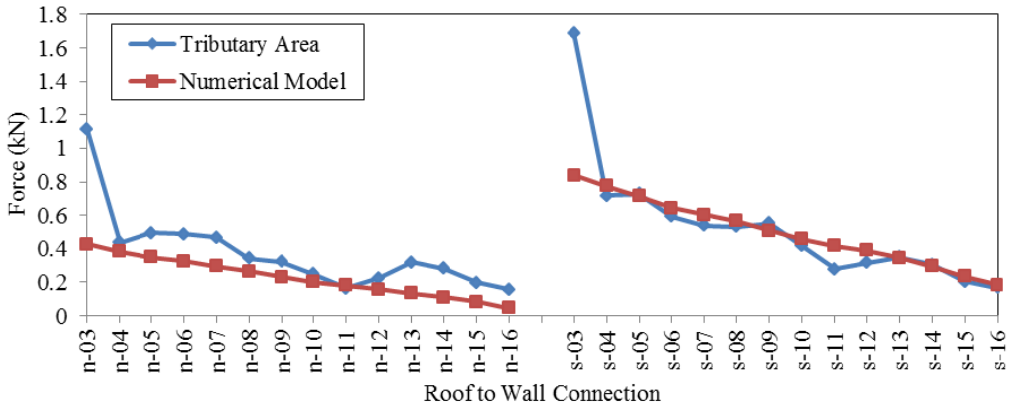

Fig. 14 RTW connection force for tributary area method and numerical model, load case 12

The numerical model tends to predict smaller forces in the connections on the interior trusses of the structure due to the increased load transferred through the gable ends. Due to this additional load shared to the gable truss, the force in every north connection is overestimated by the tributary area method for the selected pressure distribution.

Tables 3 and 4, which present the uplift force withheld by the RTW connections of the east gable truss for the 12 selected load cases, show that the numerical model predicts that the gable truss transfers much more uplift load to the walls than predicted by the tributary area method. The largest difference between the two analysis methods is under the pressure distribution applied in load case 5, where the tributary area method predicts that the dead load of the east gable truss is larger than the applied uplift load. Due to the load sharing demonstrated under this pressure distribution, the numerical model predicts that an uplift force is transferred to the walls by the RTW connections of the gable end. For the load cases analyzed from the 25 m/s experiment, the numerical model predicts that the gable end transfers 46% to 94% more uplift force than the tributary area method prediction.

Table 3 Total uplift force transferred by the RTW connections of the east gable for load cases selected from 20 m/s wind speed experiment

Load Case	1	2	3	4	5	6
Tributary Area Prediction (kN)	2.2	1.7	1	2.9	-0.1	3.7
Finite-Element Prediction (kN)	3.1	2.4	2.3	4.4	1	5.1
Percent Increase	45%	45%	135%	54%	1158%	38%

Table 4 Total uplift force transferred by the RTW connections of the east gable for load cases selected from 25 m/s wind speed experiment

Load Case	7	8	9	10	11	12
Tributary Area Prediction (kN)	2.8	2.8	2.3	2.8	2.8	3.9
Finite-Element Prediction (kN)	4.6	4.8	4.5	4.5	4.2	5.6
Percent Increase	64%	70%	94%	61%	51%	46%

The tributary area method is not capable of capturing either the load sharing that occurs in the truss system or the effect of the increased stiffness of the gable end truss. The tributary area method is most accurate in sections of the house with a uniform truss stiffness without large variation in loading from truss to truss. The inability of the tributary area method to capture the effect of the gable truss results in a very conservative force approximation for the critical connection.

5.2 Behaviour under uniform and non-uniform load

The purpose of this section is to compare the roof behaviour under a spatially varying wind load to that of an equivalent uniform pressure to gain further insight into the load sharing behaviour of the structure. Using a weighted average based on the area of each experimental pressure box, an equivalent uniform pressure is calculated for the windward and leeward sides of the structure. The equivalent uniform pressure matches the realistic pressure distribution in terms of global uplift applied to the structure. This average pressure is then applied to the numerical model for comparison with the spatially varying pressure. Load case 12 is selected for this analysis. The equivalent uniform pressure applied for this load case is -0.38 kPa on the south (leeward) side and -0.23 kPa on the north (windward) side.

Fig. 15 compares the RTW connection deflections of the structure under the realistic pressure distribution to that of the equivalent uniform pressure. Both load cases result in a similar average deflection, differing by only 5%. The peak value under the realistic pressure distribution is much higher than under the equivalent uniform loading. Both deflection and withdrawal force at the critical connection, S-03, are 80% higher under the loading of the realistic pressure distribution than under the loading of the equivalent uniform load.

Fig. 16 shows the location of the two section cuts used to draw the deflection profile of the structure under the selected pressure distributions. Section 1-1 is used to present the deflection of the top chord member of the critical truss on the leeward side of the structure. Section 2-2 is used to present the deflected shape of the sheathing along the length of the structure between the RTW connection and the nearest interior web member of the truss.

As shown in Fig. 17, the perpendicular deflection of the sheathing along the south, top chord member of the critical truss is much lower under the equivalent uniform loading than under the realistic pressure distribution, which has higher pressures acting near the eave. The maximum deflection under the realistic pressure distribution is more than double that of the equivalent uniform pressure distribution.

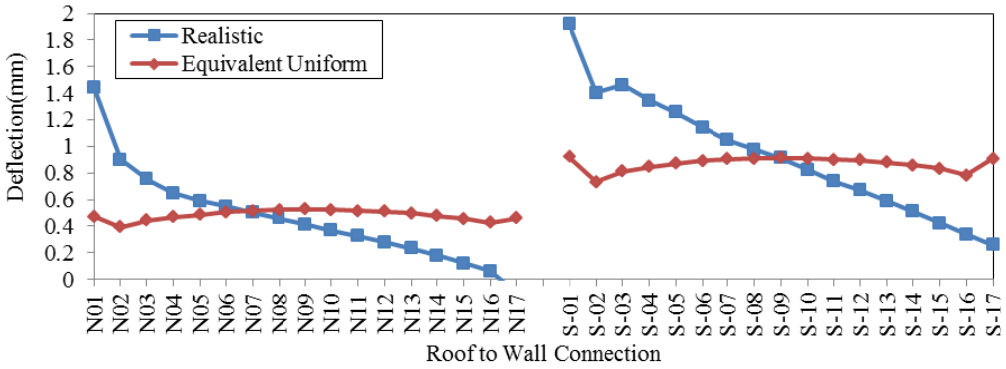

Fig. 15 RTW deflections under equivalent uniform pressure distribution and realistic pressure distribution for load case 12

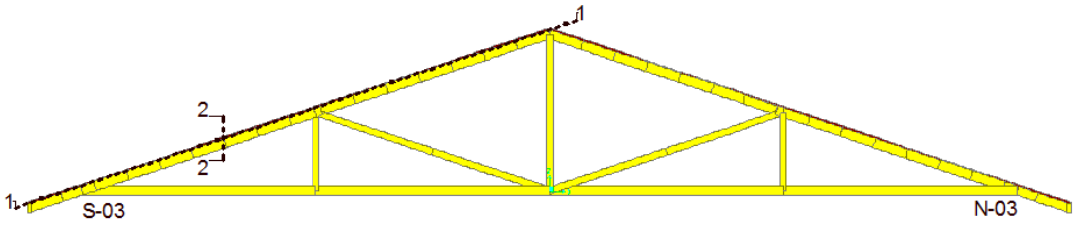

Fig. 16 Selection cuts for analysis

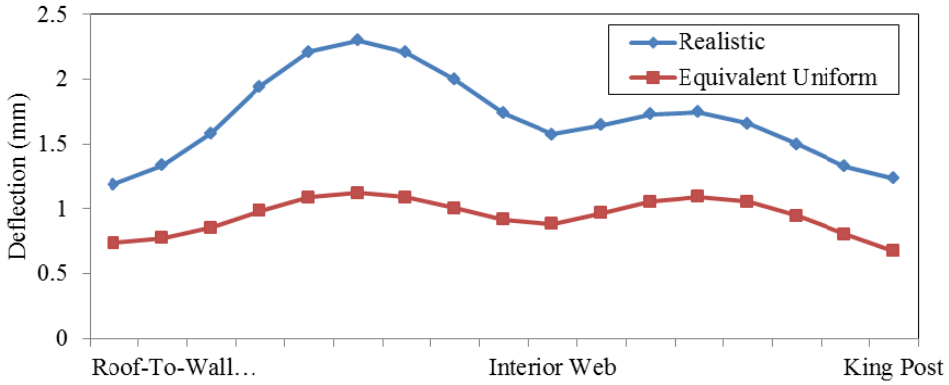

Fig. 17 Deflection profile of sheathing along section 1-1 under non-uniform and equivalent uniform pressure distribution for load case 12

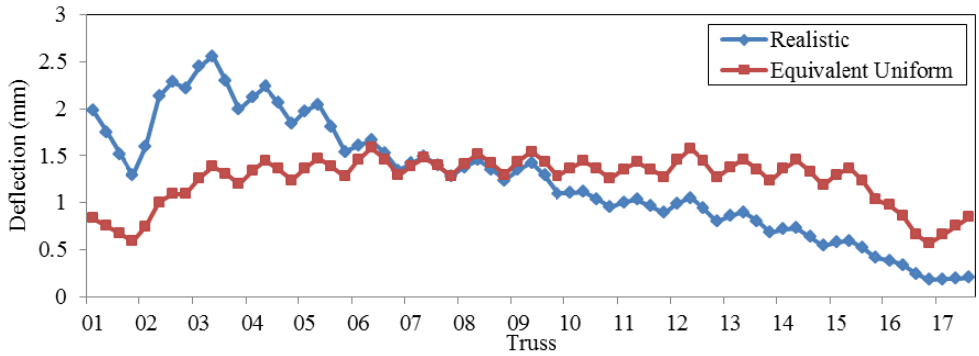

Fig. 18 Sheathing deflected profile along length of building at section 2-2 under non-uniform and equivalent uniform pressure distribution for load case 12

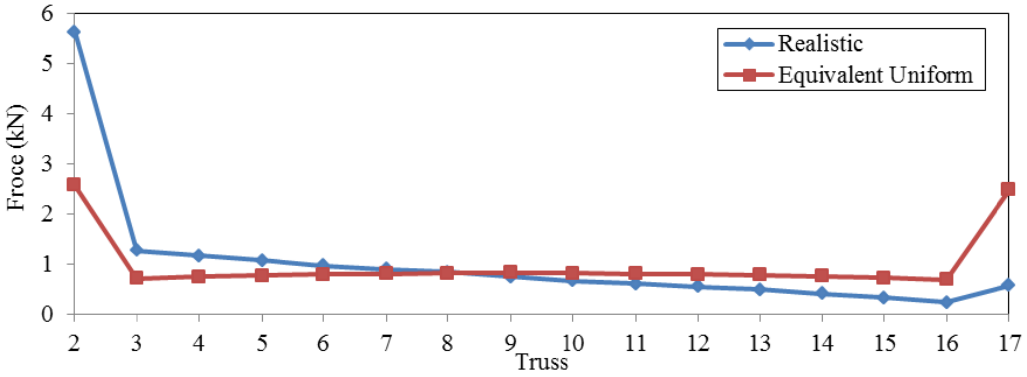

Fig. 19 Predictions of uplift force per truss under non-uniform and equivalent uniform loading

Fig. 18 presents the perpendicular deflection of the sheathing along the length of the structure at section 2-2. Local maxima occur in the sheathing between each truss. It is again found that the maximum deflection is nearly twice as large under the realistic pressure distribution than under the equivalent uniform loading.

Fig. 19 presents the sum of the force transferred by the RTW connections made between each truss and the top plate under the realistic and equivilent uniform pressure distributions. Under the realistic pressure distribution applied in load case 12, the east gable transfers 34% of the total global uplift pressure to the walls. Under the equivalent uniform pressure distribution, only 16% is transferred to the walls by the east gable end. The application of the peak pressure near the gable truss in the realistic pressure distribution allows for a larger percentage of force transfer to occur through the strong, gable truss, thereby reducing the forces on the interior RTW connections.

The equivalent uniform pressure underestimates the maximum deflections in both the sheathing and the RTW connections. The load sharing that occurs in the structure is not sufficient to create a similar behaviour between the realistic pressure distribution and an equivalent uniform loading.

5.3 Effect of increased gable end stiffness on sheathing failures

The STT connections are critical near the edges of the building where the largest pressures result from high speed winds. The results of the numerical model have identified the stiffness of the gable end to be a large factor in the uplift behaviour of the structure. The numerical model suggests extra force will be transferred by the sheathing-to-gable truss connections, increasing the vulnerability of these already critical connections.

The deflected shape of the sheathing under the non-uniform pressure distribution in Fig. 18 shows that the typical local maxima on the interior of the structure occur directly between two trusses. The local maximum between the gable truss and the first interior truss occurs closer to the interior truss than the gable truss. This location of local maximum indicates that more force is transferred through the connections of the sheathing to the more stiff gable truss. The overhang of the structure, which works as a cantilever, will also have a lower stiffness than the gable end truss. This differential stiffness in the critical location will result in the connections of the sheathing to the gable truss withstanding much more force than anticipated.

The increased demand could result in progressive overloading of the connections and removal of the roof sheathing, which has been identified as the most common failure in wood homes during high speed wind events. The effect of differential stiffness of the truss system has yet to be studied in the analysis of the failure of the roof sheathing. As the numerical model suggests unequal force transfer by the sheathing connections in this critical area, more analysis should be completed on this topic.

6. Conclusions

A finite-element model of the roof system of a light-framed wood structure is developed using the software SAP 2000. The model simulates the full-scale experiment conducted under simulated wind loading at the Insurance Research Lab for Better Homes. Frame, area and link elements are used to model the roof of the structure.

The validation of the numerical model is conducted by comparing the deflections along the length of the roof obtained numerically and experimentally under multiple realistic pressure distributions. The comparison between the full-scale test results and the finite-element analysis shows good agreement in magnitude of deflection and trend of the deflected shape. In the author's opinion, discrepancies are acceptable.

In a comparison to the numerical results, the tributary area method has not provided an accurate prediction of the loads acting on the RTW connections along the length of the structure. The tributary area method is shown to be not capable of capturing either the load sharing that occurs in the truss system or the effect of the increased stiffness of the gable end truss. The numerical model predicts that a large amount of load sharing occurs to the gable truss. For loading applied from the 25 m/s experiment, the gable truss carries between 46-94% more uplift numerically than the tributary area prediction depending on the pressure distribution. Load sharing to the gable is larger when peaks are applied closer to the gable.

A comparison of the structural behaviour under a realistic pressure distribution and an equivalent uniform pressure distribution shows that the load sharing that occurs in a wood structure is not sufficient to create a similar behaviour between the two load cases.

The behaviour in the numerical model suggests that the differential stiffness of the truss system around the gable end will increase the vulnerability of the sheathing to truss connections in the critical location. A further investigation should be completed on the effect of the increased stiffness of the gable end and the effect of this on the withdrawal failure of the STT connections.

Acknowledgments

This research has been funded by The Natural Science and Engineering Research Council of Canada (NSERC) and M. A. Steelcon Engineering Limited.

References

Baskaran, A. and Dutt, O. (1997), "Performance of roof fasteners under simulated loading conditions", *J. Wind Eng. Ind. Aerod.*, **72**, 389-400.

Canadian Wood Council (CWC) and Canadian Standards Association (CSA) (2010), *Wood Design Manual, 2010 :The Complete Reference For Wood Design In Canada*, Canadian Wood Council, Ottawa, Ontario, Canada.

Computers and Structures, Inc. (2009), *SAP 2000 V. 14: Integrated Software for Structural Analysis and Design*, Berkley, California, USA.

Datin, P.L. and Prevatt, D.O. (2013), "Using instrumented small-scale models to study structural load paths in wood-framed buildings", *Eng. Struct*., **54**, 47-56.

Datin, P.L., Prevatt, D.O. and Pang, W. (2011), "Wind-uplift capacity of residential wood roof-sheathing panels retrofitted with insulating foam adhesive", *J. Architect. Eng.*, **17**(4), 144-154.

Department of Housing and Urban Development (HUD) (1993), *Assessment Of Damage To Single-Family Homes Caused By Hurricanes Andrew And Iniki*, Office of Policy and Development and Research, United States.

FEMA (1993), *Building Performance: Hurricane InikiIn Hawaii - Observations, Recommendations, And Technical Guidance*, Federal Emergency Management Agency, United States.

Gurley, K., Davis, R.H., Ferrera, S.P., Burton, J., Masters, F., Reinhold, T. and Abdullah, M. (2006), "Post 2004 hurricane field survey – an evaluation of the relative performance of the Standard Building Code and the Florida Building Code", *Proceedings of the 2006 ASCE/SEIStructures Congress*, St. Louis, May.

Li, Z., Gupta, R. and Miller, T.H. (1998), "Practical approach to modeling of wood truss roof assemblies", *Practice Periodical Struct. Des. Constr*., **3**(3), 119-124.

Morrison, M.J. (2010), *Response of a two-story residential house under realistic fluctuating wind loads*, Ph.D. Dissertation, The University of Western Ontario, London, Ontario, Canada.

Morrison, M.J., Henderson, D.J. and Kopp, G.A. (2012), "The response of a wood-frame, gable roof to fluctuating wind loads", *Eng. Struct*., **41**, 498-509.

Morrison, M.J. and Kopp, G.A. (2011), "Performance of toe-nail connections under realistic wind loading", *Eng. Struct.*, **33**(1), 69-76.

National Research Council of Canada (NRC) (2010), *National Building Code Of Canada 2010*, National Research Council of Canada, Ottawa, Ontario, Canada.

Ontario Building Code (2006), Toronto, Ont.

Reed, T.D., Rosowsky, D.V. and Schiff, S.D. (1997), "Uplift capacity of light-frame rafter to top plate connections", *J. Architect. Eng*., **3**(4), 156-163.

Shanmugam, B., Nielson, B.G. and Prevatt, D.O. (2009), "Statistical and analytical models for roof components in existing light-framed wood structures", *Eng. Struct.*, **31**(11), 2607-2616.

Shivarudrappa, R. and Nielson, B.G. (2013), "Sensitivity of load distribution in light-framed wood roof systems due to typical modeling parameters", *J. Perform. Constr. Fac.*, **27**(3), 222-234.

van de Lindt, J., Graettinger, A., Gupta, R., Skaggs, T., Pryor, S. and Fridley, K. (2007), "Performance of wood-frame structures during Hurricane Katrina", *J. Perform. Constr. Fac.*, **21**(2), 108-116.

Zisis, I. and Stathopoulos, T. (2012), "Wind load transfer mechanisms on a low wood building using full-scale load data", *J. Wind Eng. Ind. Aerod*., **104-106**, 65-75.